Multimodality cardiac image analysis for the assessment of coronary artery disease

Gupta, V.

3

Fully automatic registration and segmentation in cardiac MR perfusion images

This chapter was adapted from:

V. Gupta, E. A. Hendriks, J. Milles, R. J. van der Geest, M. Jerosch-Herold, J. H. C. Reiber, and B. P. F. Lelieveldt.**Fully automatic registration and segmentation of first-pass myocardial perfusion MR image sequences**, *Academic Radiology*, Volume 17, Issue 11, Pages 1375–1385, 2010.

Abstract

Derivation of diagnostically relevant parameters from first-pass myocardial perfusion MR images involves the tedious and time consuming manual segmentation of the myocardium in a large number of images. To reduce the manual interaction and expedite the perfusion analysis, we propose an automatic registration and segmentation method for the derivation of perfusion linked parameters. A complete automation was accomplished by first registering misaligned images using a method based on Independent Component Analysis (ICA), and then using the registered data to automatically segment the myocardium with Active Appearance Models (AAM). We used 18 perfusion studies (100 images per study) for validation wherein the automatically obtained (AO) contours were compared with expert drawn contours on the basis of point-to-curve error, Dice index, and relative perfusion up-slope in the myocardium. Visual inspection revealed successful segmentation in 15 out of 18 studies. Comparison of the AO contours with expert drawn contours yielded 2.23 ± 0.53 mm and 0.91 ± 0.02 as point-to-curve error and Dice index, respectively. The average difference between manually and automatically obtained relative up-slope parameters was found to be statistically insignificant ($p = 0.37$). Moreover, the analysis time per slice was reduced from 20 minutes (manual) to 1.5 minutes (automatic). We proposed an automatic method that significantly reduced the time required for analysis of first-pass cardiac MR perfusion images. The robustness and accuracy of the proposed method were demonstrated by the high spatial correspondence and statistically insignificant difference in perfusion parameters, when AO contours were compared with expert drawn contours.

CONTRAST enhanced magnetic resonance imaging (MRI) techniques, such as first-pass myocardial perfusion imaging, have become an important tool for diagnosis of ischaemic heart disease. First-pass myocardial perfusion imaging involves the acquisition of MR images at the same phase during the first pass of contrast medium through heart in multiple cardiac cycles. This imaging process requires the acquisition of data over a period of 45 to 60 seconds.

The main aim of perfusion imaging is the derivation of myocardial perfusion linked parameters (e.g., relative up-slope), which requires tracking of regional myocardial intensity in all the frames of a perfusion sequence as a function of time. Because the signal must be derived from the same myocardial region in successive frames to obtain accurate results, the perfusion assessment method must include correction measures for respiratory-induced motion of the myocardium. The most commonly used approach to assess myocardial perfusion involves the manual delineation of myocardium with epi- and endocardial contours by an expert (regarded as gold standard). A typical perfusion sequence, as such, consists of 50-65 frames per slice and therefore, the task of manually segmenting the myocardium in each frame of the sequence is tedious and time consuming.

To date, several semi- and fully-automatic methods have been proposed to solve the problem of respiratory induced motion. Most of the proposed methods include intensity or model based registration for the reduction of displacement error caused by this motion. The minimization of displacement error has been performed by using registration criteria based on squared intensity differences [30], normalized cross-correlation [38, 92], mutual information [19, 36], and a measure based on gradient strength and direction [231]. A recent development in perfusion image registration has been the application of model assumptions that relate not only to the shape of the myocardium [19, 85, 231] but also to the intensity curve of the perfusion sequence [67, 86, 188]. Although these techniques have shown promising results, they are usually limited by manual interaction. In addition, only a few of the fully automatic methods have included the quantitative evaluation based on perfusion parameters [30, 68]. Another limitation is their inability to deal with the contrast variation in right ventricle (RV) and left ventricle (LV) during the first-pass of contrast bolus. This limitation was overcome by a recently proposed approach that took into account the characteristic temporal contrast variation in the perfusion sequence [154].

As suggested in the preceding discussion, a fully automatic approach, incorporating measures to deal with rapid contrast variation and ability to perform perfusion analysis, is highly desirable. The goal of this study was to develop a fully automatic framework for the analysis of cardiac MR perfusion images by extending the registration method proposed in our earlier work [154]. The proposed approach focuses on first registering the perfusion sequences and then segmenting the myocardium in the whole sequence to obtain diagnostically relevant perfusion parameters automatically.

Physiologically, a perfusion sequence can be considered as the result of a number of independent processes that contribute to the observed contrast variations [154]. The extraction of these sources of variation allows reconstruction of a spatially static reference image that can be used to align displaced frames in the perfusion sequence. Independent component analysis (ICA) has been successfully used for this type of blind source separation problems where little prior information is available about the sources. Because of its high speed and open availability, ICA was employed in the proposed method to register perfusion sequences and also to extract the information for subsequent

segmentation in the registered sequence.

Although the myocardial displacement is significantly reduced by ICA based registration, the automation of myocardial segmentation continues to pose challenges due to the presence of (a) noise and artifacts introduced during image acquisition, (b) papillary muscles and other anatomical structures around left ventricle, and (c) low contrast between the myocardium and surrounding tissues. Therefore, the segmentation method should integrate prior knowledge on myocardial appearance. Our method employs active appearance models (AAMs) [57] to delineate myocardial boundaries, since they allow the incorporation of prior knowledge on myocardial shape and texture. Furthermore, the task of initializing AAM contours and selecting an optimal contrast image is performed by utilizing the information from the components, which are extracted for the ICA based registration.

There are, primarily, three contributions that we propose in this work:

1. We improved the registration strategy proposed in [154] by adding another registration pass at full resolution and by performing the constrained expansion of the search space for LV matching in order to reduce large shifts of perfusion images within a slice.

2. A segmentation method based on AAM was integrated in the registration strategy to identify and delineate the myocardium in registered images without requiring user interaction. For the complete automation of the perfusion analysis pipeline, the initialization of the AAM based segmentation was performed by utilizing the components from ICA.

3. A validation of the fully automatic registration and segmentation pipeline was performed on the basis of point-to-curve error, Dice index and perfusion related parameters.

3.1 Background

3.1.1 Independent Component Analysis (ICA)

ICA is a source separation method, which aims to represent non-Gaussian data linearly in such a way that the essential structure of the observed data can be captured with only a few statistically independent component sources S and their corresponding weights W [55, 136]. Let an image with size $p \times q$ from the perfusion sequence be represented in vectorized form as:

$$I = [g(x_1, y_1), g(x_1, y_2), g(x_1, y_3), ..., g(x_p, y_q)]^T \tag{3.1}$$

and the complete perfusion sequence with n time points as:

$$X = [I_1 I_2 I_3 ..... I_n]^T \tag{3.2}$$

where, I_t represents images at time points $t = 1, 2, 3, ..., n$. In the form of an ICA model, the observation space (a perfusion sequence) can be shown as:

$$X = \bar{X} + WS \tag{3.3}$$

where $S \in \Re^{k \times pq}$ consists of independent components, k is the number of retained components and pq represents the size of perfusion images. The matrix $W \in \Re^{n \times k}$ in Equation 3.3 defines the weight coefficients representing the time-intensity variation of k component images and n is the number of frames per slice of the perfusion sequence. The linear combinations of the component images contained in S and the corresponding

coefficients in W provide approximations of the original frames and are referred to as reference frames. Due to its blind source separation properties, ICA has been used successfully to solve time sequence based problems in various image processing and medical image analysis applications [43, 45, 106].

3.1.2 Active Appearance Model (AAM)

AAMs were proposed by Cootes et al.[57] in 1998 and, since then, they have found widespread use in various image segmentation applications [33, 70, 156, 157, 226, 228].

3.1.2.1 Model Building

AAMs rely on the fact that an object's variability can be learned from a training set by building an appearance model that integrates shape and texture (pixel intensities) information. To this end, the expected shape is drawn on all the images in the training set by annotating them with landmark points corresponding to the same location in each image. For our application, a shape is defined by P two-dimensional landmark points and is represented as: $s = [x_1, y_1, x_2, y_2, ..., x_P, y_P]^T$. Because the sample shapes in different training images can vary in scale and orientation, Procrustes analysis [90] is performed to compensate for these variations. The shape model is built using the mean shape and the shape related modes of variation, which are obtained by applying principal component analysis (PCA) on the sample covariance matrix. The model thus obtained (Equation 3.4) can be used to generate a new shape instance s.

$$s = \bar{s} + Q_s b_s \tag{3.4}$$

Here, $\bar{s}$ is the mean shape, Q_s consists of shape eigenvectors and b_s are the model deformation parameters.

In contrast to the shape modeling where landmarks in the shape vectors constitute the data itself, the texture modeling requires a consistent method for collecting the texture information between the landmarks. The texture model is, therefore, built by warping gray values into correspondence using a piece-wise affine warp, which is normalized and sampled from the Procrustes aligned mean shape. In order to avoid the influence from the global linear changes in pixel intensities, the warping is followed by a photometric normalization of the texture vectors t of the training set. Hereafter, akin to the shape model construction process, PCA is performed on the training image textures to find the texture related modes of variation (Q_t) and the mean texture vector for the texture model:

$$t = \bar{t} + Q_t b_t \tag{3.5}$$

where $\bar{t}$ is the mean texture and b_t are the texture related model deformation parameters. The parameter vectors b_s and b_t summarize the shape and texture of any sample from the training dataset. To recover the correlation between shapes and textures, we apply PCA on the concatenated vector:

$$b_c = \begin{pmatrix} W_s b_s \\ b_t \end{pmatrix} \tag{3.6}$$

which, based on Equations 3.4 and 3.5, can also be written as:

$$b_c = \begin{pmatrix} W_s Q_s^T (s - \bar{s}) \\ Q_t^T (t - \bar{t}) \end{pmatrix} \tag{3.7}$$

where W_s is a diagonal matrix that consists of weight factors for the shape parameters. The PCA on the combined vector b_c yields another model:

$$b_c = Q_a a \tag{3.8}$$

where Q_a represents appearance eigenvectors and a represents appearance parameters that controls both the shape and the texture of the model. The use of simple linear algebra yields the expression for generating shape and texture instances in terms of combined model parameters, a:

$$s = \bar{s} + Q_s W_s^{-1} Q_{as} a \tag{3.9}$$

$$t = \bar{t} + Q_t Q_{at} a \tag{3.10}$$

where,

$$Q_a = \begin{pmatrix} Q_{as} \\ Q_{at} \end{pmatrix} \tag{3.11}$$

The model thus obtained gives a compact representation of the permissible variations in the appearance (shape and texture) as seen in the training set and allows the synthesis of a sample image for a given a by generating the shape-free texture image from the vector, t, and warping it using the control points described by s.

3.1.2.2 Model Matching

The AAM matching makes use of the model built in training step (previous section) to know what is expected in the unknown (target) image, and typically attempts to find the best model parameters which generate a model instance as close as possible to the target image (perfusion testing data).

For a set of model parameters, a, we generate an instance of the model projected into the target image and compare it with the target image to get an error measure which, in our case, is the root mean square between the current model instance and the target image. The best set of parameters to interpret the objects in the target image is then the set which minimizes this error measure. To generate model instances, we employ an iterative approach that involves incremental additive updates to the shape and appearance parameters. With an initial estimate of shape parameters, the target images are warped onto the model co-ordinate frame thus allowing us to obtain the root mean square error between the current model instance and the target image. The error thus obtained is minimized by repeating the update of model parameters using a gradient descent approach until convergence. The model parameters obtained after the convergence provide the best fitting model instance and can be used for further processing, such as for measurement or classification. In the proposed method, these parameters yield the best possible endo- and epicardial contours for the target images.

3.2 Data

3.2.1 AAM Training Data

The images in the training dataset were acquired using 1.5T Philips Gyroscan NT Intera MR Scanner with a 5-element Synergy coil during breath-holds. The electrocardiogram gating was used to obtain images of the same phase during a cardiac cycle. The heart was imaged from apex to base with 10 to 12 imaging slices in the short-axis orientation.

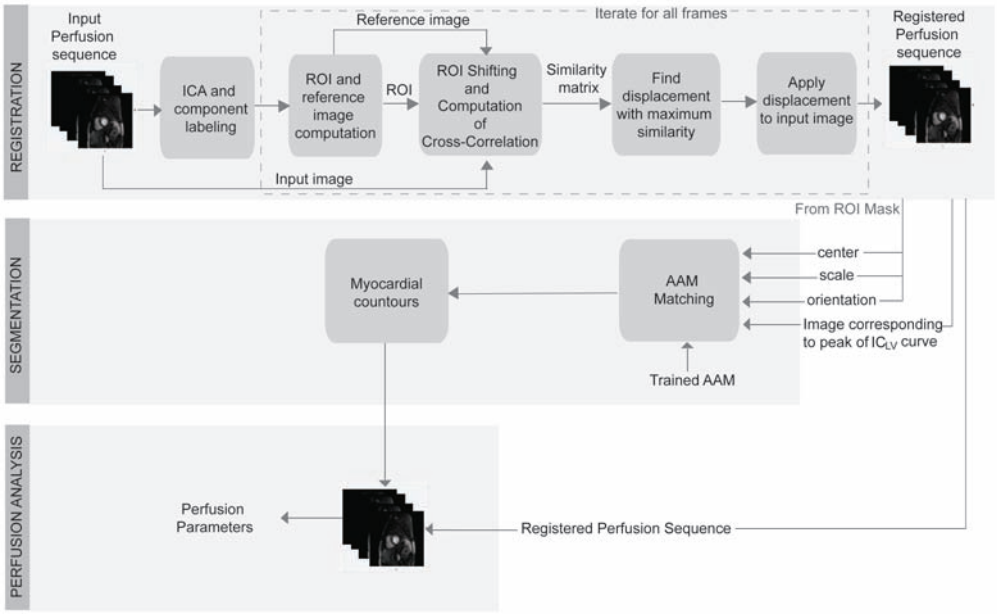

Figure 3.1: Overview of the proposed method

Typical imaging parameters were 400 x 400 mm^2 Field-of-View, 10mm slice thickness, 256 x 256 image resolution and 1.5mm pixel size. A subset of 50 images was selected randomly to include considerable shape and texture variability in the AAM.

3.2.2 Perfusion Testing Data

The validation data used for the proposed algorithm consisted of 18 rest MRI datasets that were obtained for the multi-ethnic study of atherosclerosis (MESA) [31]. The selected datasets comprised three slices per dataset and 50 frames per slice. Because only mid-ventricular and basal slice ground truth contours were available, our dataset for validation consisted of 100 frames per dataset. All the images were acquired with a Siemens Sonata(1.5T) MR scanner using a fast gradient echo pulse sequence (TR 2 ms, TE 1.2 ms, flip angle 18°) and T1-weighting. For each study, three slices were obtained (pixel size: 1.37 1.37 mm , slice thickness: 8 mm, slice gap: 8 mm) in short-axis orientation. The breathhold period of 12-18 s was used during acquisition and a Gadolinium-DTPA (Gd-DTPA) bolus (Magnevist, Berlex, Wayne, NJ) of 0.04 mmol/kg of body weight was injected, starting at the third or fourth heartbeat, followed by a saline flush of 10 mL. The first pass of the injected contrast agent bolus through the right and left ventricles and its first recirculation was captured in 50 heartbeats.

3.2.3 Ground truth contours

The manual segmentation of the myocardium in perfusion testing data was performed by two experts (designated as Observer A and Observer B) using the MASS software [246].

3.3 Methods

An overview of the proposed method is shown in Figure 3.1. As shown in the figure, this method consists of two parts: the ICA based registration and the AAM based segmentation phase. The registration part takes a perfusion sequence with misaligned images as input and provides a set of parameters and a registered sequence as output for segmentation. Both steps are described in following subsections:

3.3.1 ICA based Registration

A time-intensity analysis of a typical perfusion sequence provides three physiologically important components viz., a right ventricle component (IC_{RV}), a left ventricle component (IC_{LV}), and a baseline component (IC_{BL}). These components are assumed to be the main sources contributing to the dynamic behaviour of whole perfusion sequence, and their extraction, using ICA, is based on the contrast variability induced by the passage of a contrast agent through heart. It has been shown in a study by Milles et al. that ICA is able to separate these components with a high accuracy in most cases [154].

Computation and labeling of components: ICA is performed on the complete perfusion sequence and feature images viz., IC_{RV} (right ventricle), IC_{LV} (left ventricle), IC_{BL} (baseline), IC_{MC} (myocardium), IC_{BM} (breathing motion), representing events occurring during the perfusion sequence, are extracted. Their signs are determined by the signs of their mean values. The labeling of these feature images is based on a majority voting system of the parameters such as mean weight value, maximum weight value, time point of maximum, histogram symmetry and maximum time derivative, which are derived from the weighting curves corresponding to feature images [154].

Computation of the region of interest (ROI) and reference image: The left ventricle (LV) is identified and localized by coarsely segmenting the LV blood pool using a thresholding function on the IC_{LV} image. The LV mask (ROI) is then computed as the rectangle that encompasses the LV completely by ensuring that its outermost pixels fall within the LV radial extent. The LV radial extent, rad_{LV}, is obtained by computing the distance between the blood pool centres of LV and RV. To obtain the reference image, it is essential to identify and label the components correctly. However, it was observed that the correct identification and labeling of the component corresponding to myocardium (IC_{MC}) was difficult to achieve due to the low myocardial signal intensity in several images. As a result, only the components IC_{RV}, IC_{LV}, and IC_{BL} that were reliable with respect to the identification and labeling were used for the computation of reference image. The component corresponding to the breathing motion (IC_{BM}) is considered as noise and is, hence, not used in the reference image computation. Figure 3.2 depicts the weighting curves and feature images corresponding to IC_{RV}, IC_{LV} and IC_{BL} for one slice. A reference image for each frame is then defined by the linear combination of selected component images and corresponding coefficients in the weight matrix (Equation 3.3).

Computation of the displacements and alignment of frames: Each frame in the sequence is aligned using a rigid registration after comparing it with the reconstructed reference image for that frame. The ROI calculated in the last step allows reduction of computation time by restricting the search area. We compute cross-correlation between the ROI in

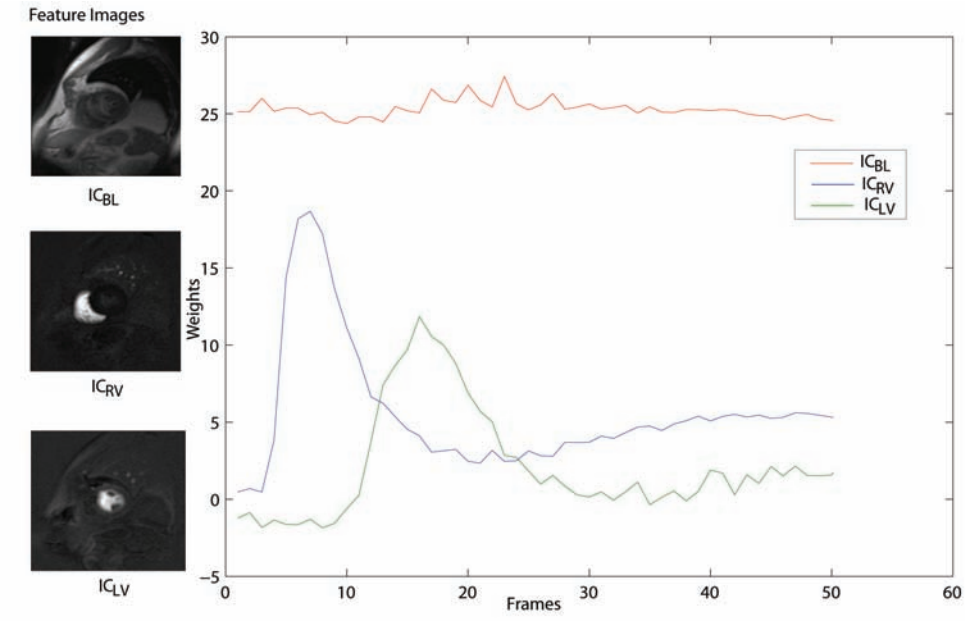

Figure 3.2: A typical example showing weighting curves and the feature images obtained after the application of ICA

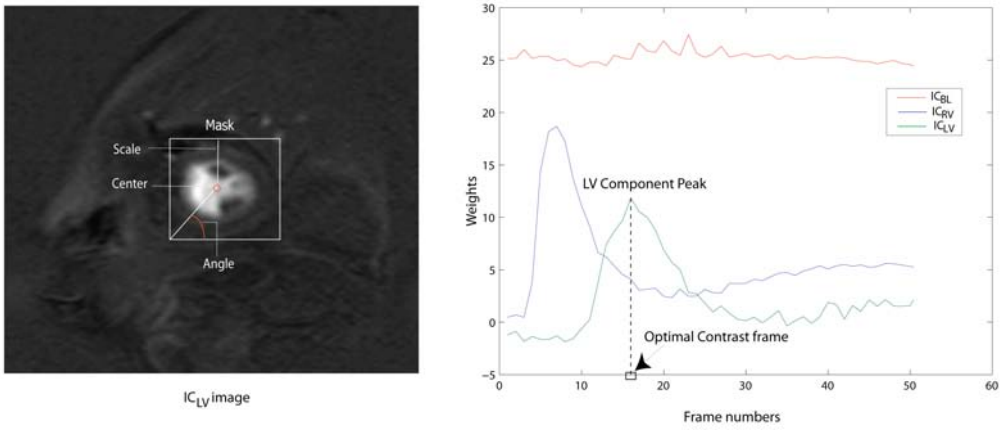

Figure 3.3: Extraction of initial parameters from the components derived from ICA: The scale, center, and orientation angle for the initialization of AAM contour are calculated from the LV mask. The optimal contrast frame for the AAM based segmentation is indicated by the peak of LV weighting curve.

reference and input images in order to find the similarity matrix by shifting the ROI over a specified displacement range. Due to the similarity in intensity distribution between the reconstructed reference images and the input images, cross-correlation was found to be a

highly robust and rapidly computable measure for obtaining the similarity matrix. The images in the input dataset are then aligned with their respective reference images by applying the displacement based on the maximum value from the similarity matrix.

All the registration steps can be repeated in multiple passes because the use of multi-resolution passes mitigates the effect of motion on the computation and labeling of independent components. Moreover, the multi-resolution strategy also saves computation time as shown by Milles et al.[154] who used first pass of coarser (sub-sampled by two) resolution and one pass of full resolution. However, it is often the case that the acquisition process of perfusion sequences results in extremely large movements of diaphragm during rapid breathing motion. We observed that the addition of one more pass of registration at full resolution provided a significant improvement in case of large shifts. Therefore, we added one more iteration of registration at full resolution to the earlier method [154] in order to offset those large displacements. Furthermore, the search space was expanded by increasing the range of displacements by 33% for shifting ROI to compute the similarity matrix.

3.3.2 AAM based Segmentation

Segmentation utilizes a priori information of shape and intensity by employing trained AAM contours (refer to *Model building* section) to delineate myocardial borders in registered images. The following sections describe how AAM matching is used in the proposed method:

Derivation of initialization parameters: The performance of AAM matching depends considerably on the selection of three initialization parameters: position, orientation and scale of the AAM contours. We derive these parameters from the ICA based registration. The angle between the diagonal and the inferior edge of the mask serves as the initial orientation and rad_{LV} obtained during registration, contributes the initial scale of AAM contour. Figure 3.3 depicts how the initial parameters are derived from ICA components.

Selection of the optimal contrast frame for segmentation: For the myocardial segmentation, the registration step is followed by the selection of an optimal contrast image from the registered set. Automation of the selection process is accomplished by selecting the image corresponding to the IC_{LV} peak frame as it provides a high contrast between myocardium and surrounding tissue. In order to use a model contour for segmentation, AAM building (refer to section *Model Building*) is used once on the training data prior to the application of the proposed method. The model contour thus obtained is then applied on the selected image using the initialization parameters. Based on the *Model Matching* method described earlier, the desired myocardial contours are obtained for further analysis after convergence.

3.3.3 Validation Indices

We evaluated the effectiveness of the proposed method by comparing the ground truth contours with the automatically obtained contours (AO contours) on the basis of following:

3.3.3.1 Spatial correspondence

To test the spatial correspondence of automatically obtained contours with ground truth contours, we used point-to-curve errors and Dice indices. The point-to-curve error is calculated as the Euclidean distance from AO contours to ground truth contours. The Dice index, which indicates extent of overlapping area between ground truth and AO contours, is calculated as the area of intersection between ground truth and AO contours divided by the mean of individual contour areas as shown in Equation 3.12:

$$\text{Dice index} = 2\frac{|P \cap Q|}{|P| + |Q|} \tag{3.12}$$

where P and Q represent the areas corresponding to the overlapping contours.

3.3.3.2 Myocardial perfusion analysis

We used absolute and relative up-slope parameters for the semi-quantitative assessment of myocardial perfusion due to their wide acceptance as reliable indices [8, 112]. The absolute up-slope of myocardium is given by the maximum value of the first-derivative of myocardial time-intensity curve during the initial ascent of the first pass. The absolute up-slope of myocardium is then normalized by the absolute up-slope of LV pool to obtain relative up-slope parameter.

3.3.4 Statistical Analysis

To determine whether the automatically obtained perfusion parameters differ significantly from the manually obtained parameters, a paired samples t-test was performed at 95% significance level under the assumption that the paired differences are independent.

3.3.5 Implementation details

A PC with Intel(R) Core(TM)2 Duo CPU @ 2.6 GHz and 2GB RAM was used for the execution of the implemented method. Both the proposed method and the validation experiments were implemented using MATLAB® [1].

3.4 Results

A visual inspection of the segmentation results revealed that the proposed method succeeded in identifying and delineating correct myocardial region in 15 out of 18 studies. A further analysis showed that, out of 36 slices in the perfusion testing dataset, segmentation failed in 2 slices (both slices in one patient study, as shown in Figure 3.4) and registration was unsuccessful in 4 slices (both slices in 2 patients).

As shown in the Figure 3.5a, the ICA driven initialization of AAM contours was able to successfully locate myocardium in the optimal contrast image. Figure 3.5b depicts the final contours obtained after the convergence of AAM matching. A visual comparison of ground truth and AO contours is shown in Figure 3.6. The point-to-curve errors, obtained by the proposed method and existing methods, are provided in Table 3.1. These values show an improvement of 24% and 35% over the methods proposed by Stegmann et al.[226] and Ólafsdóttir et al.[171], respectively. Table 2 summarizes the point-to-curve errors separately for endo- and epicardial contours with respect to mid-ventricular and basal slices. A similar analysis is shown on the basis of Dice index in Table 3.3. Boxplots depicting the spread of the point-to-curve error and Dice index are shown for all the studies in Figure 3.7.

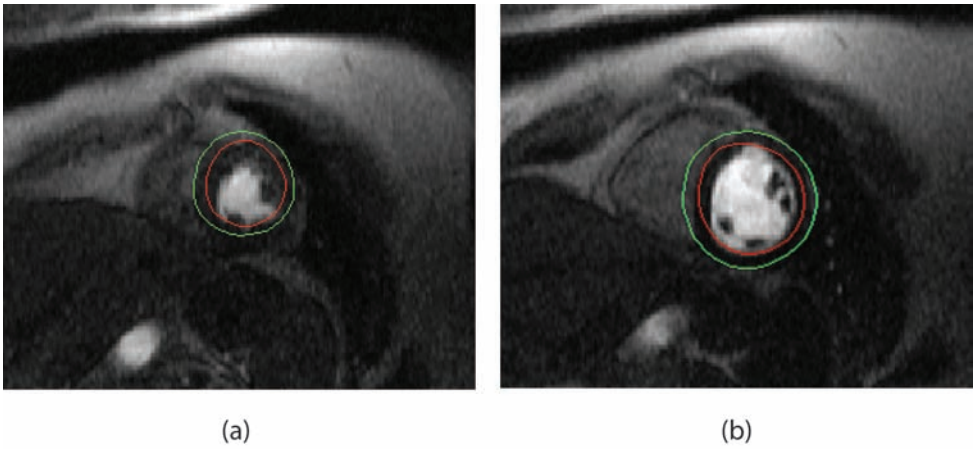

Figure 3.4: AAM Matching failure in (a) Mid-ventricular slice and (b) Basal slice of same patient study

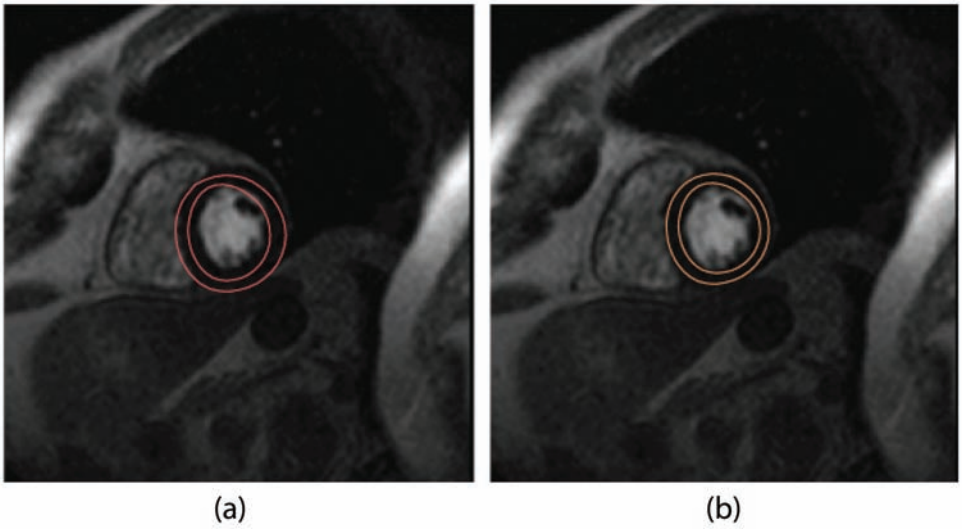

Figure 3.5: AAM contours (a) before and (b) after the AAM matching

To study the incursion of LV and RV blood pools into the myocardial region, we present an analysis of the differences in signal intensities within the regions enclosed by AO and ground truth contours: Figure 3.8 depicts the intensity variation w.r.t. frames and Figure 3.9 shows the intensity variation w.r.t. slices (mid-ventricular and basal). The results of perfusion analysis are presented in Table 3.4, which also includes p-values from paired samples t-test. The Bland-Altman plot in Figure 3.10 further shows the agreement between manual segmentation and the proposed method by comparing the mean and

Table 3.1: A comparison of existing methods with the proposed method based on point-to-curve error (in mm)

Methods	Mean ± Std. dev. (mm)
Proposed method	2.23 ± 0.56
Stegmann et al.[226]	2.93 ± 0.84
Ólafsdóttir et al.[171]	3.44 ± 1.73

difference of absolute up-slope parameter.

For each slice consisting of 50 frames, it took our method altogether 1.5 minutes on average to register all the frames, to obtain myocardial contours, and to derive perfusion parameters.

3.5 Discussion

The presented results show the potential of a fully automated framework for the analysis of cardiac MR perfusion images. When compared to the manual gold-standard, the proposed method achieved a high spatial correspondence and similar values for the diagnostically relevant perfusion parameters albeit within a fraction of time required by manual segmentation; the automatic method took 1.5 minute per slice for the myocardial segmentation as opposed to 20 minutes required for manual segmentation, thereby reducing the analysis time by more than 92%. This large reduction in analysis time is, mainly, due to the employment of ICA because it allows the extraction of physiologically significant components such as IC_{RV}, IC_{LV}, and IC_{BL} for registration, and initialization parameters for AAM based segmentation, thus facilitating the full automation of myocardial perfusion analysis.

3.5.1 Spatial correspondence

The automatically obtained myocardial contours were occasionally found to be over- (in case of epicardial contour) and underestimation (in case of endocardial contour) of the corresponding manual contours. This is as expected because, while the automatic method delineates myocardium along the edges in images, the manual contours are drawn well within the myocardial boundaries to avoid incursions of pixels from RV and LV blood pools into the myocardium. However, our results on perfusion analysis suggested that a little deviation in size of contours does not strongly affect the derivation of perfusion parameters, if the automatically obtained contours accurately enclose only myocardium. Table 3.2 and Figure 3.7(a-b) provide an indication of the point-to-curve distance variability after the proposed method was applied on perfusion testing data. The epicardial contours tend to have higher error and spread than endocardial contours since the epicardial boundaries are usually not easily discernible. However, these errors do not have a significant impact on the clinically relevant perfusion parameters as shown in Table 3.4. Moreover, the two sets of contours compared reasonably well w.r.t. Dice index (Table 3.3, 3.7(c-d)). The inter-observer point-to-curve error and Dice index measurements were only slightly better than the corresponding values obtained by the proposed method. A further comparison of AO contours with contours from observer A and B suggested that values w.r.t. observer A were closer to inter-observer difference. This observation can be ascribed to the similarity in the fashion in which contours were obtained by the proposed method and observer A i.e., one set of contours was obtained for only one phase

Table 3.2: Point-to-curve distance measurements (in mm) obtained from the comparison of manual contours from observers A and B with automatically obtained (AO) contours. The last column shows inter-observer measurements. All values in the table are shown in the format: mean ± standard deviation.

Comparisons	**Obs. A vs. AO**		**Obs. B vs. AO**		**Obs. A vs. Obs. B**	
Contours	Endocardial	Epicardial	Endocardial	Epicardial	Endocardial	Epicardial
Mid-ventricular Slice	2.44 ± 0.53	2.55 ± 0.71	2.90 ± 0.68	3.08 ± 0.98	1.77 ± 0.57	2.08 ± 0.75
Basal Slice	1.71 ± 0.53	2.55 ± 0.46	2.50 ± 0.62	2.51 ± 0.58	1.76 ± 0.49	2.02 ± 0.71

Table 3.3: Dice index measurements obtained from the comparison of manual contours from observers A and B with automatically obtained (AO) contours. The last column shows inter-observer measurements. All values in the table are shown in the format: mean ± standard deviation.

Comparisons	**Obs. A vs. AO**		**Obs. B vs. AO**		**Obs. A vs. Obs. B**	
Contours	Endocardial	Epicardial	Endocardial	Epicardial	Endocardial	Epicardial
Mid-ventricular Slice	0.89 ± 0.02	0.91 ± 0.02	0.87 ± 0.03	0.88 ± 0.04	0.91 ± 0.03	0.93 ± 0.03
Basal Slice	0.92 ± 0.02	0.93 ± 0.01	0.90 ± 0.02	0.92 ± 0.02	0.93 ± 0.02	0.93 ± 0.02

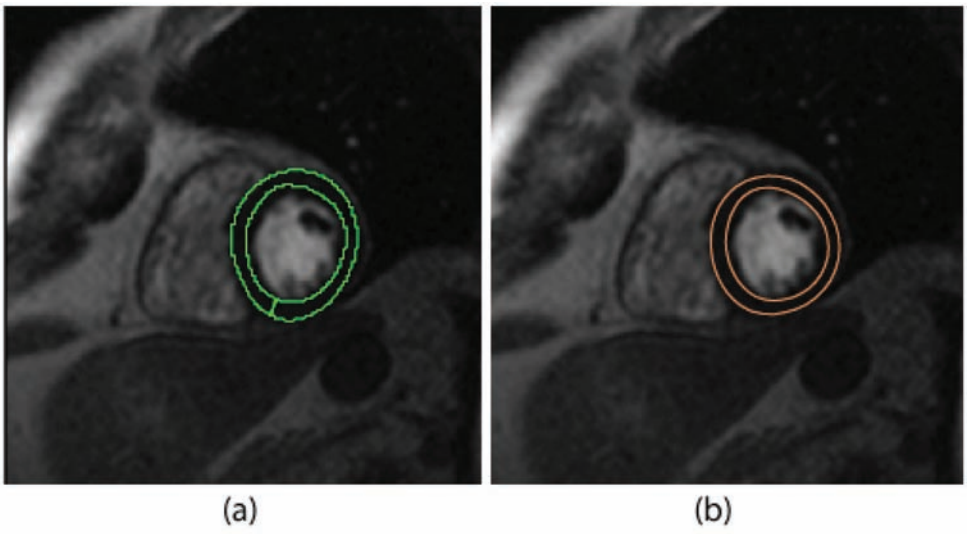

Figure 3.6: Visual comparison of (a) Ground truth contours with (b) AO contours

of each slice followed by its propagation to other phases along with minor translations, if required. Observer B segmented individual frames of each slice adapting to rigid as well as non-rigid transformations.

It is worth noting that the proposed method succeeded in identifying and delineating desired myocardial regions despite the fact that the AAM training and the matching were performed on datasets acquired using disparate protocols and MR scanners from different

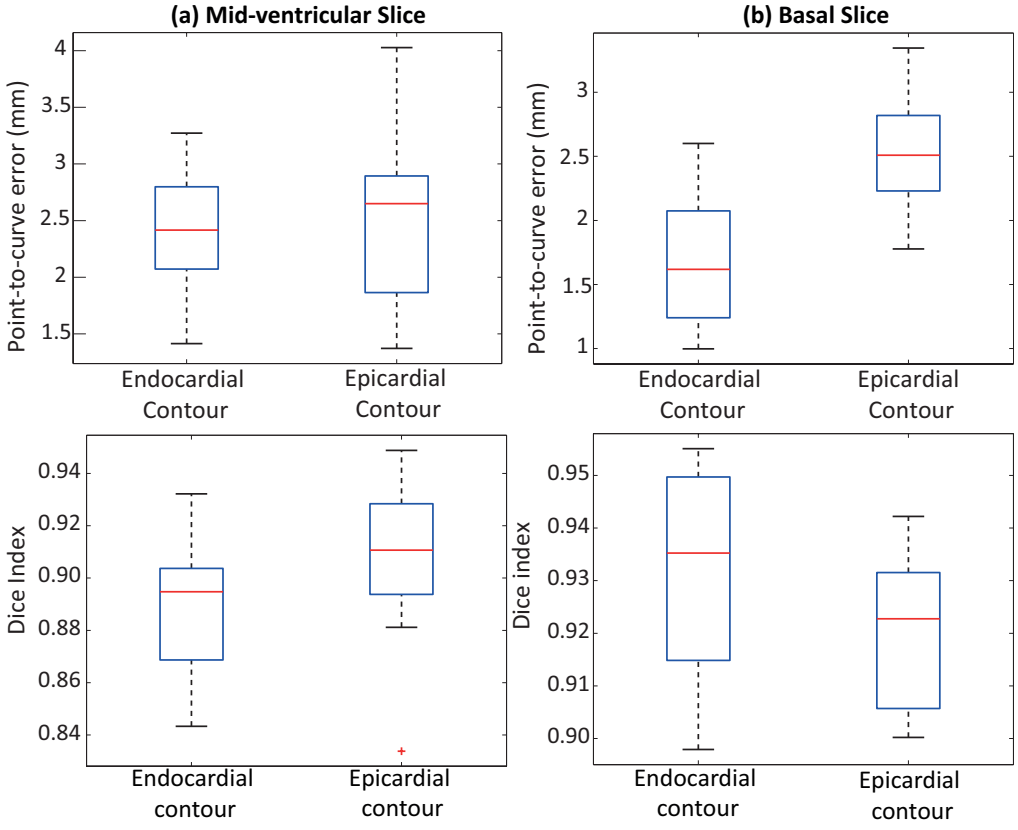

Figure 3.7: Boxplot showing point-to-curve errors and Dice index for all the datasets: plots in column (a) represent mid- ventricular slices, and plots in column (b) represent basal slices.

vendors; the data for AAM training consisted of MR function scans from Philips scanner, and the model thus obtained was used for AAM matching on perfusion testing data that consisted of MR perfusion images from Siemens scanner.

3.5.2 Myocardial perfusion analysis

The results on relative and absolute up-slope differences give an indication of the suitability of the proposed method in a clinical set up. As shown in Table 3.4, the differences between the values obtained manually and automatically were found to be statistically insignificant ($p=0.37$ for relative up-slope and $p=0.12$ for absolute up-slope). The standard deviation of relative up-slope parameters for the complete dataset remained unchanged when it was computed with the proposed method, and the further analysis of absolute up-slope values (Figure 3.10) for all slices suggests that there is little to no variation in the values obtained manually and automatically. In the Bland-Altman plot (Figure 3.10), the distribution around the mean suggests the absence of both a systematic error and a visible trend. The intensity distribution shown in Figures 3.8 and 3.9 indicated that both AO and ground truth contours enclosed the same myocardial region. As shown in both figures, the

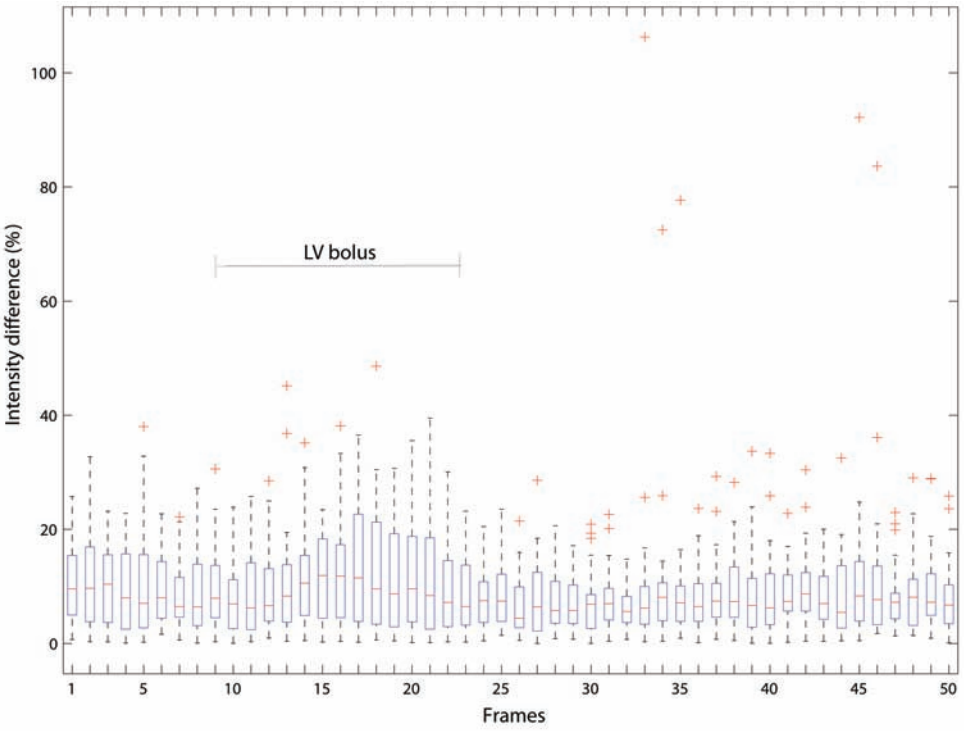

Figure 3.8: Difference (in percent) between the Ground truth and AO contour intensity curves for all frames of the complete dataset

variation of differences is significantly lower and only a few outliers are indicated in Figure 3.8 during the first-pass (frame 1 through 35) as compared to the second-pass (frame 36 through 50) of contrast agent. These observations indicate that the proposed method does well to avoid the incursions of pixels from LV blood pool into the myocardium, thus suggesting its suitability for regular use in clinics.

Table 3.4: Up-slope parameter obtained using the Ground truth and AO contours for the complete dataset

Parameter	Ground truth contours	AO contours	p value
Relative up-slope	0.11 ± 0.08	0.11 ± 0.08	0.37
Absolute up-slope	0.40 ± 0.13	0.38 ± 0.13	0.26

3.5.3 Limitations

The accurate segmentation of the myocardium in the proposed method relies primarily on the ICA's ability to identify and label correct components, hence, an identification and labeling failure in few cases translates to the incorrect contour application on misregistered frames. This failure of registration can be attributed to the poor quality of images and a large breathing motion during image acquisition. As an implication of this failure, it was no longer feasible to propagate one set of contours to all the frames of the perfusion

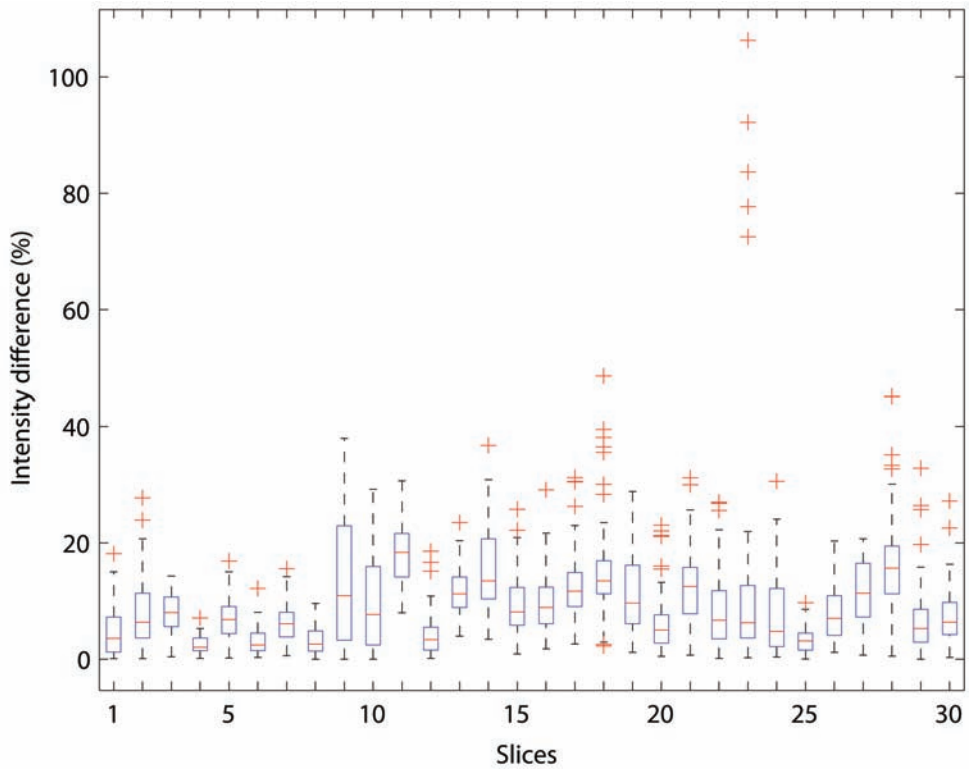

Figure 3.9: Difference (in percent) between the Ground truth and AO contour intensity curves for all slices of the complete dataset

sequence since it contradicted our basic assumption that, post registration, myocardium should be located at same position in all the frames. The segmentation failure (Figure 3.4) was observed mainly in those images that had higher myocardial shape variability with respect to the training shapes. Therefore, we ascribe these failures to the limitations of trained AAMs that prohibit the model from deforming according to the edge-information in a few images. However, this issue can be resolved in the future by training the AAM with more shapes and images, extending the shape variability of the model.

3.5.4 Future perspectives

We intend to direct the current work towards the improvement of registration strategy to reduce unusually large and rapid breathing motion that affects the identification and labeling of correct components. In addition, training of AAM with a larger pool of shapes and images will make the segmentation more robust. Finally, the clinical validation should be extended to multi-vendor datasets and, more importantly, to the images of the patients with pathological conditions in order to demonstrate the true potential of the proposed method.

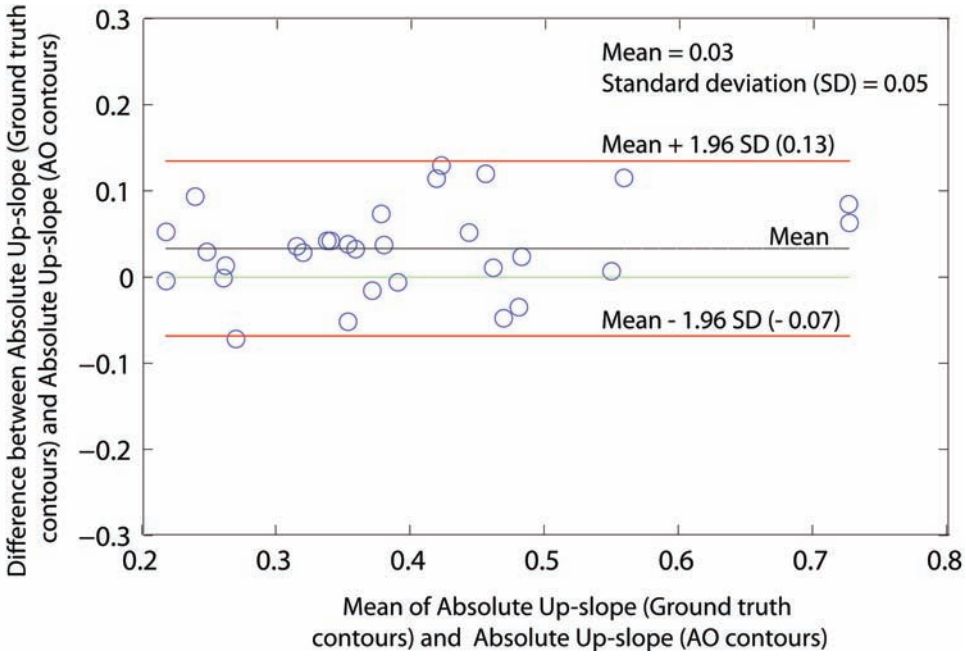

Figure 3.10: Bland Altman plot comparing the absolute up-slope parameters obtained from the Ground truth and AO contours for the complete dataset

3.6 Conclusion

We proposed an integrated registration and segmentation pipeline that is completely automatic and hence, very fast compared to manual methods. The complete automation and rapid processing were accomplished by first registering misaligned images using a method based on ICA, and then using the output of the registration step to automatically segment the myocardium with AAM. The results related to point-to-curve distance and overlap area, for a dataset comprising 1500 images, indicated that our method achieved a high spatial correspondence with the manual gold standard. Furthermore, the analysis based on myocardial time-intensity curve demonstrated that the difference between manually and automatically obtained perfusion parameters was statistically insignificant. With the presented results, we have shown the potential of the proposed method in accelerating the analysis of first-pass cardiac MR perfusion image sequences.

3.7 Acknowledgment

The contributions of personnel involved in MESA study (http://www.mesa-nhlbi.org) are gratefully acknowledged. We would also like to thank Avan Suinesiaputra for his suggestions during the preparation of this manuscript.